THE JOURNAL OF BIOLOGICAL CHEMISTRY VOL. 282, NO. 7, pp. 5004–5014, February 16, 2007
Printed in the U.S.A.

Inhibition of Metalloprotease Botulinum Serotype A from a Pseudo-peptide Binding Mode to a Small Molecule That Is Active in Primary Neurons*[S]

Received for publication, August 24, 2006, and in revised form, October 20, 2006 Published, JBC Papers in Press, November 8, 2006, DOI 10.1074/jbc.M608166200

James C. Burnett[‡], Gordon Ruthel[§], Christian M. Stegmann[¶], Rekha G. Panchal[‡], Tam L. Nguyen[‡], Ann R. Hermone[‡], Robert G. Stafford[§], Douglas J. Lane[‡], Tara A. Kenny[‡], Connor F. McGrath[‡], Peter Wipf[‖], Andrea M. Stahl[§], James J. Schmidt[§], Rick Gussio[**], Axel T. Brunger[¶1], and Sina Bavari[§2]

From the [‡]Target Structure-based Drug Discovery Group, SAIC-Frederick, Inc., and the [**]Information Technology Branch, Developmental Therapeutics Program, National Cancer Institute-Frederick, Frederick, Maryland 21702, the [§]United States Army Medical Research Institute of Infectious Diseases, Fort Detrick, Frederick, Maryland 21702, the [¶]Howard Hughes Medical Institute (HHMI) and Departments of Molecular and Cellular Physiology, Neurology and Neurological Sciences, and the Stanford Synchrotron Radiation Laboratory, Stanford University, School of Medicine, Stanford, California 94305, and the [‖]Combinatorial Chemistry Center, University of Pittsburgh, Pittsburgh, Pennsylvania 15260

An efficient research strategy integrating empirically guided, structure-based modeling and chemoinformatics was used to discover potent small molecule inhibitors of the botulinum neurotoxin serotype A light chain. First, a modeled binding mode for inhibitor 2-mercapto-3-phenylpropionyl-RATKML (K_i = 330 nM) was generated, and required the use of a molecular dynamic conformer of the enzyme displaying the reorientation of surface loops bordering the substrate binding cleft. These flexible loops are conformationally variable in x-ray crystal structures, and the model predicted that they were pivotal for providing complementary binding surfaces and solvent shielding for the pseudo-peptide. The docked conformation of 2-mercapto-3-phenylpropionyl-RATKML was then used to refine our pharmacophore for botulinum serotype A light chain inhibition. Data base search queries derived from the pharmacophore were employed to mine small molecule (non-peptidic) inhibitors from the National Cancer Institute's Open Repository. Four of the inhibitors possess K_i values ranging from 3.0 to 10.0 μM. Of these, NSC 240898 is a promising lead for therapeutic development, as it readily enters neurons, exhibits no neuronal toxicity, and elicits dose-dependent protection of synaptosomal-associated protein (of 25 kDa) in a primary culture of embryonic chicken neurons. Isothermal titration calorimetry showed that the interaction between NSC 240898 and the botulinum A light chain is largely entropy-driven, and occurs with a 1:1 stoichiometry and a dissociation constant of 4.6 μM.

Botulinum neurotoxins (BoNTs)[3] are the most potent of the biological toxins (1), and are listed as category A (highest priority) bioterror agents by the Centers for Disease Control and Prevention. They may be delivered by aerosol route (1, 2), and consequently represent a serious threat to both military personnel and civilians (3, 4). Moreover, BoNTs are now established biotherapeutics for a range of physical ailments and cosmetic treatments (2, 5–8), making their misuse and/or adverse side effects (9) more likely. Neither the currently available BoNT antitoxin nor antibodies can counter these toxins once they are inside neurons; currently, critical care mechanical ventilation is the only life-saving treatment option. However, the effects of internalized BoNTs can last for months (10), and mechanical ventilation would be impractical if even a limited number of individuals were clandestinely/accidentally intoxicated. Thus, there is an urgent need to identify and develop small molecule (non-peptidic) inhibitors (SMNPIs) that can serve as both prophylactics and post-exposure therapeutics.

BoNTs are composed of a heavy chain and a light chain (LC) that are connected by a disulfide bridge (11). The heavy chain binds to neurons and transports the LC into the cytosol (12). The LC is a zinc metalloprotease. Each of the seven BoNT serotypes (A–G) cleaves a component of the SNARE (soluble NSF-ethylmaleimide-sensitive factor attachment protein receptor) proteins (13), which mediate the exocytosis of acetylcholine into neuromuscular junctions. BoNT serotypes A and E cleave

* The work was supported by Defense Threat Reduction Agency Grant 3.10024_06_RD_B, 2S.Bavari, the United States Army Medical Research and Material Command, and IAA Y3 CM 100505 (MRMC and NCI, National Institutes of Health). This project has been funded in whole or in part with federal funds from the National Cancer Institute, National Institutes of Health, under Contract N01-CO-12400. This research was supported (in part) by the Developmental Therapeutics Program in the Division of Cancer Treatment and Diagnosis of the NCI. The costs of publication of this article were defrayed in part by the payment of page charges. This article must therefore be hereby marked "*advertisement*" in accordance with 18 U.S.C. Section 1734 solely to indicate this fact.

[S] The on-line version of this article (available at http://www.jbc.org) contains additional Methods, Results and Discussion, references, Figs. S1–S4, and Tables S1–S2.

The atomic coordinates and structure factors (code 2ISE, 2ISG, and 2ISH) have been deposited in the Protein Data Bank, Research Collaboratory for Structural Bioinformatics, Rutgers University, New Brunswick, NJ (http://www.rcsb.org/).

[1] To whom correspondence may be addressed: HHMI and Depts. of Molecular and Cellular Physiology, Neurology and Neurological Sciences, and Stanford Synchrotron Radiation Laboratory, Stanford University, School of Medicine, 318 Campus Dr., Rm. E300, Stanford, CA 94305. Tel.: 650-736-1031; Fax: 650-736-1961; E-mail: brunger@stanford.edu.

[2] To whom correspondence may be addressed: United States Army Research Institute of Infectious Diseases, 1425 Porter St., Fort Detrick, Frederick, MD 21702. Tel.: 301-619-4246; Fax: 301-619-2348; E-mail: sina.bavari@us.army.mil.

[3] The abbreviations used are: BoNT, botulinum neurotoxins; SMNPI, small molecule (non-peptidic) inhibitors; LC, light chain; SNAP, synaptosomal-associated protein; SAR, structure-activity relationship.

SNAP-25 (synaptosomal-associated protein (25 kDa)) (14), serotypes B, D, F, and G cleave VAMP (vesicle-associated membrane protein, also referred to as synaptobrevin) (15–18), and serotype C cleaves both SNAP-25 and syntaxin 1 (19). Recently, it was shown that sequence variability exists within serotypes, and that this subtype variability can have an impact on antibody binding and neutralization (20).

The most potent, lowest molecular weight pseudo-peptide inhibitor of BoNT serotype A LC (BoNT/A LC) metalloprotease activity was generated over the course of two investigations (21, 22). In the first, a substrate-based approach was used to generate CRATKML (K_i = 2 μM) (22). In the second, derivatives were generated, and 2-mercapto-3-phenylpropionyl-RATKML (mpp-RATKML) (Table 1) was found to possess a K_i = 330 nM (21). An extensive structure-activity relationship (SAR) study was performed on this inhibitor (Table 1) (21).

In this study, we docked mpp-RATKML in the BoNT/A LC substrate binding cleft to map out potential new steric volume and intermolecular interactions for SMNPIs. The conformer of the bound pseudo-peptide was used to: 1) refine our pharmacophore for BoNT/A LC inhibition; and 2) generate search queries that were used to mine potent SMNPIs of the BoNT/A LC from the National Cancer Institute's Open Repository. One of the identified inhibitors displays dose-dependent protection of SNAP-25 in a primary culture of embryonic chicken neurons.

EXPERIMENTAL PROCEDURES

Molecular Modeling—All molecular modeling was performed on a Silicon Graphics Octane 2. Insight II (Accelrys, San Diego, CA) was used to build and inspect models. Energy refinement and molecular dynamics were performed using the Discover and Discover 3.0 programs (Accelrys) and the cff91 force field. The HINT (hydropathic interactions) program (eduSoft, Richmond, VA) was used to evaluate model quality based on the quantitation of intra- and intermolecular contacts (23) (supplemental Refs. 1–5 provide additional descriptions of the HINT program). HINT parameter settings: steric term = Lennard-Jones 6–9 (for cff91 compatibility); lone pair vector focusing = 10; and distance dependence atom-atom interactions = exp ($-1/r$). Figures for molecular models were generated using Insight II and Catalyst 4.7 (Accelrys).

Conformational sampling of mpp-RATKML was performed using a previously described molecular dynamics protocol (24). In brief, the objective was to sample a sufficient volume of conformational space to determine whether mpp-RATKML and/or its derivatives (from Table 1) utilized the preorganization of molecular substituents to facilitate binding in the BoNT/A LC substrate cleft. An equilibration phase using direct velocity scaling for 10 ps was followed by 100 ps of dynamics using the Berendson method of temperature-bath coupling. The temperature was increased by 25° increments from 0 K to the simulation temperature of 300 K. A sample structure was collected every 100 fs. A distance dielectric of 1.0 was used. The 100 lowest energy conformers from the trajectory were examined for preorganizational intramolecular contacts and BoNT/A LC substrate cleft compatibility.

The x-ray crystal structure of the BoNT/A LC that was used for enzyme coordinates: Protein Data Bank code 1E1H (25); resolution = 1.8 Å. Energy refinement and molecular dynamics protocols for 1E1H have been described previously (26, 27). The coordinates of the energy-refined model of 1E1H were within its experimentally determined x-ray crystallographic resolution. For root mean square deviation comparisons between the energy-refined dynamics conformer of 1E1H and its corresponding x-ray crystal structure see supplemental materials "Methods." For the x-ray co-crystal of SNAP-25 residues 146–204 in complex with the BoNT/A LC (PDB code 1XTG (28), resolution = 2.1 Å), mutated residues (28) Gln-224 and Phe-366 were restored to Glu and Tyr, respectively. Energy refinement performed on the 1XTG co-crystal followed the same methods as described for 1E1H.

During mpp-RATKML docking, ranges for the S–zinc interaction distance and angle of incidence were 2.1–2.4 Å (29, 30) and 98–112° (29), respectively. The manual docking of each inhibitor component involved translational, rotational, and torsional adjustments, as well as torsional adjustments to enzyme residue side chains (within acceptable limits defined by rotamer libraries). A van der Waals bump of 0.25 Å was used to remove unacceptably close atom-atom contacts. A tethered minimization strategy was used during model refinement. The strategy involved the application of 2000 kcal/mol per Å^2 of force that was stepped off the inhibitor-protein model in 100 kcal/mol decrements by minimizing with conjugate gradients until the norm of the gradient was 0.001 kcal/Å. This process was repeated until all external force was removed. Following, inter- and intramolecular analyses of the docked inhibitor were performed using the HINT program (23), and unfavorable interactions were removed using rounds of manual adjustments (translational, rotational, and torsional) and tethered minimizations. This optimization cycle was repeated until a binding mode meeting all of our requirements was achieved. Finally, the inhibitor-enzyme complex was saturated with an 8.0-Å thick shell of water molecules. Hydrogens only were minimized until the gradient of the norm was 0.001 kcal/Å, and then the entire complex (enzyme, inhibitor, and water molecules) was again energy refined (until the gradient of the norm was 0.001 kcal/Å) to give the final model.

Search query generation and compound library data base mining was performed using Catalyst 4.7 (Accelrys). The "best flexible" search mode was used for all data base screens. The molecular docking of SMNPIs was performed using the tethered minimization protocol described for mpp-RATKML.

Assay of BoNT/A LC Protease Activity—The assay for BoNT/A protease activity was carried out as previously described (21, 22, 31, 32). K_i values for the inhibitors were calculated from the slopes of Dixon plots with the equation: $K_i = K_m/(\text{slope} \times V_{\max} \times \text{S})$, where S is the substrate concentration (33). Each value is the average of two independent determinations, using nine concentrations of inhibitor in each. In all cases, standard deviations were less than ±25%.

Neuronal Cell Cultures—Embryonic chicken spinal motor neurons were cultured by the method described in detail by Kuhn (34). In brief, fertilized chicken eggs (SPAFAS/Charles River Laboratories, North Franklin, CT) were incubated at 37 °C for 6 days. Embryos were removed from the eggs and ventral spinal cords were isolated from the embryos. Cells were

dissociated by trypsinization and trituration. Cells were preplated into a culture dish with Dulbecco's modified Eagle's medium plus 10% fetal bovine serum for 1 h to allow non-neuronal cells to attach to the dish, thereby increasing the percentage of neuronal cells in the suspension. Cells were centrifuged and resuspended in Leibovitz L15 medium (Invitrogen) with N3 supplement and 10% fetal bovine serum. The mitotic inhibitor 5-fluorodeoxyuridine was added to further reduce the population of non-neuronal (*i.e.* dividing) cells. Cells were plated into 6-well tissue culture plates that were coated first with poly-L-lysine, then with laminin. Cultures were incubated overnight at 37 °C prior to intoxication.

Microscopy—Autofluorescence was used to examine inhibitor entry into cells. Chick spinal motor neurons were incubated for 30 min with 20 μM inhibitor and examined for an increase in intracellular fluorescence on an inverted Nikon TE300 microscope with a standard 4′,6-diamidino-2-phenylindole filter set. Images were collected with a Bio-Rad Radiance 2000MP confocal/multiphoton system (Zeiss, Thornwood, NY). For confocal images used to assay morphological indicators of general cell health after toxin and inhibitor treatments, spinal motor neuron cultures were fixed for 30 min in 3.7% formaldehyde and permeabilized in 0.2% Triton X-100 for 10 min. After blocking for 30 min in 1% bovine serum albumin, cells were incubated with 1:500 DM1A anti-α-tubulin (Sigma). Cells were then labeled with 1:500 Alexa 488-conjugated goat anti-mouse secondary antibody, 1:25 Texas Red phalloidin, and Hoechst stain (Molecular Probes, Eugene, OR).

Intoxication, Inhibitor Treatment, and Western Blot Analysis—Cells were preincubated with inhibitor for 45 min, followed by 3.5 h incubation with 10 nM BoNT/A (MetaBiologics Inc., Madison, WI) and inhibitor. Cells were rinsed with fresh culture medium, scraped, collected, washed with phosphate-buffered saline, lysed, and assessed for protein content using the Bradford protein assay (Bio-Rad). Cell lysates were run on a 12% Tris glycine gel (Invitrogen), transferred to nitrocellulose, and probed with SMI 81 mouse anti-SNAP-25 (Sternberger Monoclonals Inc., Lutherville, MD), and mouse anti-glyceraldehyde-3-phosphate dehydrogenase (Covance Research Products, Inc., Berkeley, CA) primary antibodies. A horseradish peroxidase-conjugated goat anti-mouse secondary antibody was used (Pierce) in combination with an ECL Western blotting detection system (Pierce). Densitometry was performed using a UN-SCAN-IT gel automated digitizing system (Silk Scientific, Inc., Orem, UT).

Isothermal Titration Calorimetry—Purified BoNT/A LC was subjected to a final gel filtration step (Superdex 200 column) to ensure a complete buffer exchange, as well as to exclude trace amounts of autocleavage products. All experiments were carried out in the same buffer to control for heat of dilution effects: 50 mM Hepes (pH 7.4) supplemented with 150 mM NaCl and 0.5 mM $ZnCl_2$. Concentrations of NSC 240898 solutions were confirmed by UV-visible absorbance measurements. Calorimetric titration was performed multiple times on a VP-ITC calorimeter (MicroCal, Northhampton, MA) at 293 K. BoNT/A LC was used at a concentration of 28 μM in the isothermal titration calorimetry cell and inhibitor NSC 240898 at a concentration of 390 μM in the injection syringe. Prior to the titration, the samples were degassed for 10 min. The positive deflections observed at the end of the titration (Fig. 7) reflect the enthalpy of dilution of the inhibitor solution and were subtracted from the binding data. The first injection systematically showed a decreased enthalpy due to the technical limitations of the instrument and was omitted from curve fitting. The titration curve was then fit to a single site model by non-linear least squares regression as implemented by MicroCal Software Inc. in the Origin software package. According to this model, the parameters to be determined are: the number of binding sites (N), the binding enthalpy per site (ΔH), and the binding constant (K_d).

RESULTS AND DISCUSSION

The pseudo-peptide mpp-RATKML is a potent (K_i = 330 nM (21)), specific, and competitive inhibitor of the BoNT/A LC. Due to its size, diverse composition, and the extensive amount of empirical structure-activity data available for this compound, it was an ideal candidate for molecular docking studies. Indeed, a rational binding mode for this inhibitor could be used to identify new intermolecular contacts and map available steric volume within the BoNT/A LC substrate cleft. This information could then be used to refine our pharmacophore for BoNT/A LC inhibition (26, 27), allowing for the generation of new three-dimensional search queries to chemoinformatically "mine" novel SMNPIs from virtual compound databases. However, the conformational flexibility of mpp-RATKML (see Table 1 for the two-dimensional structure) represented a major challenge. Therefore, a comprehensive, biochemically realistic strategy for docking was established to ensure that the model: 1) was consistent with empirical data; 2) followed the fundamental principles of structural biochemistry (*i.e.* the hydrophobic effect, π stacking, etc.); and 3) adhered to our hydrophobicity-first rule of molecular docking, which formed the basis of our previous successes in a number of targets (for a detailed description of the hydrophobicity first rule, see supplemental "Methods").

A Dynamic Conformer of the BoNT/A LC Was Necessary for Generating an mpp-RATKML Binding Mode That Rationalized the Inhibitor SAR—An energy refined x-ray structure of the BoNT/A LC with the highest available resolution (PDB code 1E1H (25); resolution = 1.8 Å) was initially used for enzyme coordinates. However, even with parameters set for the S-zinc interaction (see "Experimental Procedures"), exhaustive molecular modeling studies failed to generate an mpp-RATKML:BoNT/A LC binding mode that satisfied our docking criteria. For example, all feasible binding conformations of the pseudo-peptide failed to rationalize its SAR, empirical data indicated a >1000-fold loss in potency for a Lys substitution (mpp-**K**ATKML) (which is normally considered to be a conservative Arg replacement) (Table 1). Nevertheless, in our binding models of the inhibitor with the energy refined x-ray structure of the BoNT/A LC a Lys replacement was feasible, the cationic side chain Nϵ of the Lys could still engage in the same interactions as the Arg guanidinium, and therefore could not account for the SAR.

Our inability to identify an acceptable binding mode for mpp-RATKML led to a pivotal question: is it possible that the

conformation of the x-ray determined BoNT/A LC may not be the bioactive conformation, at least with respect to inhibitor binding? There is evidence suggesting that this is the case (22, 31, 32, 35–38) (see supplemental "Results and Discussion"). For example, a molecular dynamics study (26) demonstrated that both a BoNT/A LC extracted from the holotoxin (PDB code 3BTA (11); resolution = 3.2 Å) and the 1E1H (25) x-ray crystal structure displayed very similar surface loop reorientations (loop 1 = residues 48–78 and loop 2 = residues 167–180) toward the substrate binding cleft. In doing so, these loops decreased the solvent accessibility of the cleft and formed potential new complementary binding surfaces for SMNPIs (26). However, α-helices and β-sheets of the LCs remained virtually unchanged (26). Likewise, a comparison of different crystal forms of the BoNT/A LC revealed that all show variation in the indicated surface loops, whereas core secondary structures for all were identical (see supplemental "Results and Discussion"). Key to our docking studies was the identification of a BoNT/A LC conformer allowing for a structure-based rationalization of the complete loss in potency that is observed for replacement derivative mpp-**K**ATKML (Table 1).

When examining a dynamics trajectory for 1E1H (25) we found that loop 1 reorientation toward the substrate binding cleft creates a hydrophobic pocket composed of the aliphatic methylenes of Lys-165 and the side chains of Val-67 and Pro-68; however, it was not until we explored the preorganizational state of mpp-RATKML that we fully understood the significance of this pocket. Specifically, the nearest local minimum for the pseudo-peptide indicated that the Arg side chain guanidinium may engage in an intramolecular cation-π interaction (39) with the mpp phenyl (Fig. 1*A*). This conformation allowed the guanidinium Nϵ to form an intramolecular hydrogen bond with the backbone carbonyl oxygen of the Ala of the inhibitor (40) (Fig. 1*A*). The cation-π interaction, in combination with the intramolecular hydrogen bond, provided: 1) an Arg side chain conformation with good steric and hydropathic complementarity for the hydrophobic pocket (described above) presented by the dynamic conformer, thus allowing for hydrophobic collapse/desolvation (Fig. 1*B*); and 2) an Arg orientation with the guanidinium of the residue facing the polar contact region of the enzyme (26, 27), thus requiring few torsional adjustments during inhibitor translation from the solvent into its proposed binding site in the substrate cleft of the enzyme (Fig. 1*B*).

For comparison, the preorganizational conformation of mpp-**K**ATKML, as expected, revealed that the Lys Nϵ might also engage in a cation-π interaction with the mpp phenyl (Fig. 1*C*); however, in contrast to the Arg guanidinium, the Lys Nϵ faces the opposite direction (Fig. 1*C*). Furthermore, its side chain methylenes adopt a reverse conformation (Fig. 1*C*) compared with those of the Arg (Fig. 1*A*). Indeed, the conformational requirements imposed by the mpp component on the Lys would force this residue to bind in the substrate cleft of the enzyme with its hydrophobic side chain methylenes pointed toward charged residues in the polar contact region (26, 27); simultaneously, its cationic Nϵ would point into the loop 1 hydrophobic pocket presented by the dynamic conformer. Such unfavorable interactions are not observed in high-resolution x-ray structures, as they impose an insurmountable entropic penalty. This is further enforced by the formation of a critically unfavorable hydrophobic-polar clash when mpp-**K**ATKML is docked via superimposition on the optimized mpp-RATKML·BoNT/A LC complex (Fig. 1*D*). Thus, these results provide a plausible explanation for the inactivity of mpp-**K**ATKML.

The final model of mpp-RATKML docked in the dynamic conformer satisfied our docking criteria and adhered to the fundamental principles of biochemistry. Fig. 2, *A* and *B*, clearly shows good complementarity between the inhibitor and the substrate binding cleft of the dynamic enzyme conformer, and a high degree of inhibitor desolvation. Table 1 details how the final binding mode for mpp-RATKML rationalized its SAR (21) for replacement, deletion, and addition derivatives. For a detailed description of the mpp-RATKML binding mode see supplemental "Results and Discussion."

An mpp-RATKML Binding Mode Derived from the sn2: BoNT/A LC Co-crystal Structure Could Not Rationalize the SAR of the Inhibitor—Prior to completion of these studies an x-ray co-crystal structure of SNAP-25 residues 146–204 (referred to as sn2 (28)) in complex with a catalytically inactive BoNT/A LC double mutant was solved (PDB code 1XTG (28), resolution = 2.1 Å). Residues 198–203 of sn2 correspond to the RATKML portion of the pseudo-peptide, and contrary to our model, these 1XTG (28) co-crystal residues (^{198}RATKML^{203}) occupy different steric locations in the substrate cleft. As a result, residues ^{198}RATKML^{203} are too far from the catalytic engine of the enzyme to result in an mpp-^{198}RATKML^{203} model with the inhibitor thiol moiety coordinating the catalytic zinc. Nevertheless, we examined this possibility to ensure the thoroughness of this study.

Accordingly, a model of mpp-RATKML that occupied the same steric space in the substrate binding cleft as the ^{198}RATKML^{203} portion of sn2 was generated. As expected, the resulting binding mode indicated that the ^{198}RATKML^{203} residues from the BoNT/A LC:sn2 co-crystal structure occupy the substrate cleft in a manner that is incapable of rationalizing the SAR associated with the pseudo-peptide inhibitor. The bases for this conclusion were: 1) the sn2-derived mpp-RATKML sulfur atom is ~7 Å removed from the zinc (supplemental materials Fig. S1), eliminating the possibility of a S–zinc coordinate bond (21, 22); 2) the position and interactions of the Arg of the sn2 derived model cannot rationalize its SAR (21) (replacing the Arg of the inhibitor with a Lys resulted in nearly identical contacts with enzyme residues, thus providing no explanation for the >1000-fold loss in potency for the Arg → Lys replacement (Table 1); 3) the Leu side chain is partly solvent exposed, and also engages in critically unfavorable hydrophobic polar contacts that are inconsistent with the SAR (Table 1); and 4) the mpp phenyl substituent of the sn2-derived mpp-RATKML is in close proximity to the polar contact region of the substrate binding cleft and oriented toward the solvent (such binding mode characteristics are inconsistent with high quality x-ray crystal structures). Thus, our structural analyses indicate that the binding mode for residues ^{198}RAT-

TABLE 1
Structure activity data (21) and structure-based rationales for replacement, deletion, and addition derivatives of mpp-RATKML

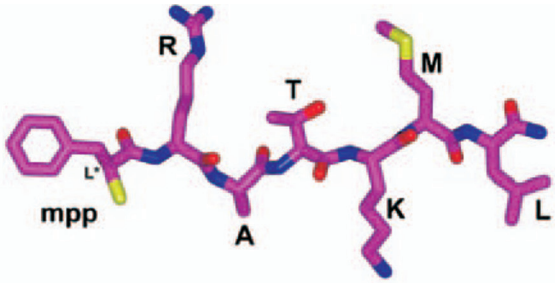

Inhibitor	K_i [a] (μM)	Rationale
mpp-RATKML	0.3	Covered in detail in the text.
Replacement derivatives		
mpp(D configuration)-RATKML	8.0	In the D configuration the mpp benzyl carbon engages in unfavorable hydrophobic-polar clashes with the side chain carboxylate of residue Glu 261, and a steric clash with the side chain tyrosyl of Tyr 365. Alleviating these unfavorable contacts would require this derivative to adopt a less optimal binding mode.
mpp-**K**ATKML	>300	Covered in detail in the text.
mpp-R**V**TKML	2.0	The original Ala side chain packs into the substrate binding cleft (Fig. 2). The bulky side chain of the Val replacement engages in hydrophobic-polar clashes with surrounding residues, resulting in a shallower binding mode.
mpp-RA**A**KML	0.7	The original Thr side chain engages in amphipathic contacts (Fig. 2). These contacts are lost upon Ala replacement, and the Ala side chain methyl points toward the solvent – increasing the entropic binding penalty.
mpp-RAT**A**ML	3.0	The original K side chain engages in favorable hydrophobic and hydrogen bonding interactions (Fig. 2). These contacts are lost upon replacement with an Ala.
mpp-RATK**A**L	0.7	The original Met residue acts as a hydrophobic anchor at the end of the substrate binding cleft (Fig. 2). Replacement with an Ala results in the loss of favorable binding contacts and a shallower binding mode.
Deletion derivatives		
mpp-R	60	The mpp sulfur interacts with the enzyme's catalytic Zn, and the phenyl substituent may still engage in favorable contacts with residues in binding subsite 1 (Fig. 2). However, the reduced size of the inhibitor, and the range of motion available to the terminal Arg would not restrict this residue to its optimal binding mode (compared to mpp-RATKML, Fig. 2). This would result in a much higher dissociation rate, and consequently weak inhibition.
mpp-RA	60	Even with the additional Ala residue, the inhibitor does not occupy enough steric space in the binding cleft to effectively compete with substrate. The latitude of motion available to this smaller inhibitor does not restrict the Arg and Ala residues to their optimal binding modes (compared to mpp-RATKML binding, Fig. 2).
mpp-RAT	30	Addition of the Thr residue brings this derivative in line with the original pharmacophore (Fig. 3*A*), and its level of potency is close to that of previously identified small molecule inhibitors (26,27). The addition of the Thr results in greater binding cleft occupancy and may aid in stabilizing optimal Arg and Ala positioning. However, a large portion of the binding cleft remains unoccupied.

TABLE 1—*continued*

Inhibitor	K_i [a] (μM)	Rationale
mpp-RATK	4	Adding the Lys residue results in the addition of favorable hydrophobic and hydrogen bonding contacts. Additionally, there is now greater binding cleft occupancy, with the length of the inhibitor approaching the cleft occupancy threshold. This serves to decrease the inhibitors dissociation rate, allowing it to compete more effectively with substrate.
mpp-RATKM	0.3	The Met reside backs up to loop 2 and packs behind Pro 238, occupying the last available steric volume in the substrate binding cleft (Fig. 2). This 'locks' the inhibitor in its most effective binding conformation. The terminal Leu residue of mpp-RATKML is not needed, as it sets on the fringe of the binding cleft (Fig. 2). Its favorable contacts with enzyme residue Val 171 are offset by entropic penalties resulting from the solvent exposure of its bulky hydrophobic side chain, as well as the flexibility of loop 2.
Addition derivative		
mpp-RATKML**GSG**	0.3	The GSG residues sit outside of the substrate binding cleft. Any favorable surface contacts and/or solvent interactions in which these residues might engage are offset by entropic penalties associated with their rotational/translational/torsional freedom.

[a] K_i values were obtained from studies conducted in Ref. 21.

KML[203] from the sn2:BoNT/A LC co-crystal cannot be used as the basis for developing an mpp-RATKML binding mode.

The mpp-RAT Portion of the Pseudo-peptide Mapped to the Pharmacophore for BoNT/A LC Inhibition—Pharmacophore components (Fig. 3*A*) were mapped to our docked conformation of mpp-RATKML to determine whether the pseudo-peptide and SMNPIs share common structural/functional group features that confer BoNT/A LC inhibition. In doing so, we found that the mpp phenyl substituent maps to pharmacophore component C (Fig. 3*B*). In previous studies (26, 27), this component was a chloro (Fig. 3*C*), methyl, methoxy, or imidazolinyl group. Furthermore, the planar-conjugated amide bonds between the mpp-R and the A-T components of the pseudo-peptide mimic pharmacophore planes A and B, respectively (Fig. 3, *A* and *B*). These planes are biaryls in reported SMNPIs (Fig. 3*C*) (27). The mpp sulfur atom corresponds to a heteroatom associated with plane A (Fig. 3, *A*–*C*), and the side chain methyl of the inhibitor Ala residue is a good match for pharmacophore component D (Fig. 3*A*, *B*), which is a chloro (Fig. 3*C*), methyl, or methoxy substituent in SMNPIs (27). Finally, the Arg guanidinium of mpp-RATKML maps to pharmacophore component E (Fig. 3, *A* and *B*), a positive-ionizable moiety that is a secondary nitrogen in SMNPIs (Fig. 3*C*) (27).

The precise match between the docked conformation of mpp-RAT and the existing pharmacophore is convincing evidence that this part of the pseudo-peptide and SMNPIs (27) are interacting with similar residues in the BoNT/A LC substrate binding cleft. Thus, it was hypothesized that incorporating additional features from the pseudo-peptide binding mode into the pharmacophore would enhance SMNPI potencies.

Hypotheses for Improving SMNPI Binding—The mpp-RATKML binding mode revealed potential new contacts and steric volume that could be used to discover/develop more potent

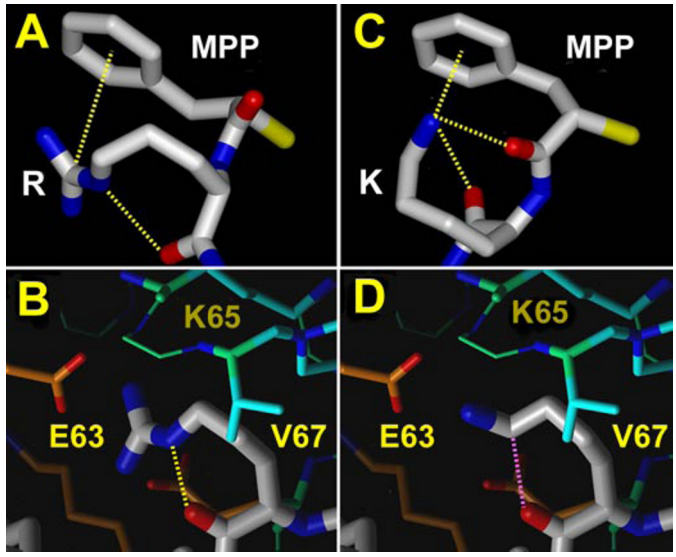

FIGURE 1. **Close-up views of mpp-RATKML and mpp-KATKML in their pre-organizational and docked conformations.** Inhibitor carbons are *white* and inhibitors are depicted in the *thicker stick*. *Yellow dashed lines* indicate hydrogen bonds and cation-π interactions; the *magenta dashed line* indicates a highly unfavorable hydrophobic-polar clash. Enzyme carbons of residues in hydrophobic binding subsite 1 (26, 27) (also referred to as the S1′ binding site (*22*)) are *cyan*, and in the polar contact region (26, 27) are *orange*. All other enzyme carbons are *green*. Nitrogen atoms are *blue*, oxygen atoms are *red*, and sulfur atoms are *yellow*. *A*, the preorganizational state of the *R*. *B*, the docked conformation of the *R*. *C*, the preorganizational state of the *K* replacement. *D*, the replacement *K* cannot bind in a manner similar to that of the *R* due to a highly unfavorable intramolecular hydrophobic-polar clash.

SMNPIs. For example, the mpp phenyl substituent (Fig. 2*A*) is a sterically and hydropathically superior match for binding subsite 1 (26, 27) (also referred to as the S'_1 binding site (22)) compared with smaller hydrophobic moieties (*i.e.* chloro, methyl, and methoxy substituents (26, 27)). This indicated that aro-

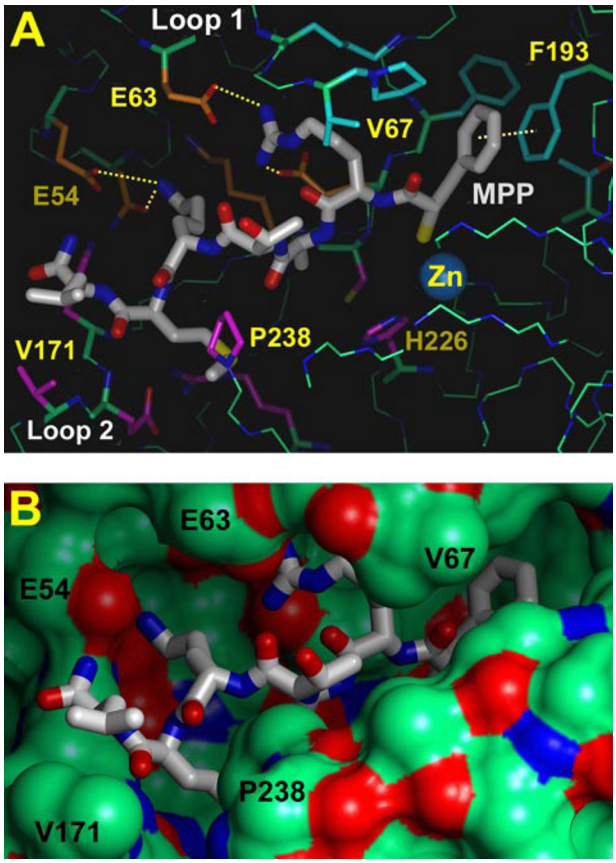

FIGURE 2. **mpp-RATKML docked in the substrate binding cleft of the molecular dynamic conformer of the BoNT/A LC.** *A*, this model adhered to our hydrophobicity first rule and our docking criteria (see "Experimental Procedures" and see supplemental "Methods"), displaying good hydrophobic and electrostatic complementarity with residues in the substrate cleft for the enzyme. *Colors* and *stick thickness* are as indicated in the legend to Fig. 1*A*, with one addition: residue carbons of binding subsite 2 (26, 27) are *magenta*. *B*, the BoNT/A LC Connolly surface. Surface colors: *green*, neutral; *red*, acidic; and *blue*, basic. mpp-RATKML is rendered in *stick* and *colors* are as indicated for *A*. Both desolvation and hydrophobic/electrostatic contacts are optimized for the inhibitor binding mode.

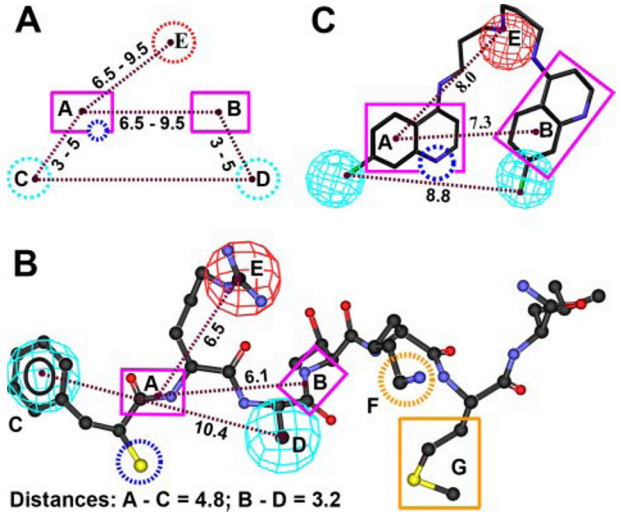

FIGURE 3. **The binding conformation of the mpp-RAT portion of the pseudo-peptide fits the common pharmacophore for BoNT/A LC inhibition, while the Lys and Met residues of the inhibitor indicate potential new pharmacophore components.** *A*, the pharmacophore for BoNT/A LC inhibition (based on previously identified SMNPIs (26, 27)). Planar components A and B are *magenta rectangles*. The *dashed*, *dark blue circle* in plane A represents a heteroatom. Hydrophobic components C and D are shown as *dashed*, *light blue circles*. The positive ionizable pharmacophore component E is shown as a *dashed*, *red circle*. *B*, Mpp-RATKML mapped to the common pharmacophore. Carbon atoms are *black*, oxygen atoms are *red*, nitrogen atoms are *blue*, and sulfur atoms are *yellow*. All pharmacophore colors are as indicated for *A*. The *orange dashed circle* and *solid rectangle* represent potential new search query components. *C*, for comparison, Q2–15 (27), a previously identified SMNPI of the BoNT/A LC (60% inhibition, 20 μM) mapped to the common pharmacophore. Q2–15 chlorine atoms are *light green*; all other colors are as indicated for *B*.

matic heterocycles or planar, conjugated guanidine/amidine/amide functional groups might also engage in favorable π-π interactions or cation-π (39, 41) interactions with Phe residues in this subsite.

The binding conformation of the Lys residue of the inhibitor identified potential new hydrogen bond contacts (Fig. 2*A*) in an area of the substrate binding cleft that has, to date, remained unexplored by our SMNPIs (26, 27) (based on our previous docking studies (26, 27)). The Lys side chain Nϵ corresponds to component F in Fig. 3*B*. Similarly, the hydrophobic anchoring position of the docked Met residue (Fig. 2*A*) indicated new contacts and steric space that might be exploited for SMNPI optimization. The Met side chain corresponds to component G in Fig. 3*B*.

Finally, empirical results from deletion/addition experiments (21) (Table 1), corroborated by data from the mpp-RATKML binding mode, suggested that there is an optimal length for BoNT/A LC inhibitors. If an inhibitor is too short (for example mpp-RAT), it does not occupy enough of the cleft, and binding affinity decreases; if it is too long (for example, mpp-RATKMLGSG), components that our model predicts will sit outside of the cleft (*i.e.* GSG) do not contribute to activity. For the docked conformation of mpp-RATKML, the distance between the mpp phenyl and the terminal Leu is ~23 Å. This distance represents an "optimal length" filter. Furthermore, to achieve this length it might be necessary to expand the distance range between pharmacophore planes A and B, to identify compounds that will occupy the full-length of the binding cleft. Additionally, amide bonds serve as mpp-RATKML pharmacophore planes. Therefore, amides, as well as bioisosteres such as alkenes, imines, and azo linkages may also serve as SMNPI pharmacophore planes.

The Identification of More Potent SMNPIs—To test the hypotheses espoused in the previous section, data base search queries were generated. An initial query incorporating all original pharmacophore components (Fig. 3*A*), in addition to the suggested components and criteria indicated above, identified no data base "hits." Consequently, a more judicious approach was adopted. This involved creating random combination search queries composed of 4 to 5 pharmacophore components. Of the numerous queries that were generated, the one identifying the four most potent inhibitors included: 1) a pharmacophore component C (Fig. 3*A*) that incorporated aromatic substituents (with and without heteroatoms), as well as planar-conjugated positive-ionizable functional groups; 2) a positive ionizable component, labeled F (Fig. 3*B*), to mimic the Nϵ nitrogen of the mpp-RATKML Lys; 3) an increased distance range between pharmacophore planes A and B (6.5–13 Å); 4) the inclusion of alkenes, imines,

amides, and azo linkages as pharmacophore planes; and 5) a compound length constraint of 23.0 Å.

Fig. 4 shows the four most potent inhibitors mapped to the search query. Interestingly, even with pharmacophore modifications, distances between planes A and B, and plane A and component C, are largely within original pharmacophore specifications (compare Figs. 3*A* and 4) for these inhibitors, further demonstrating the consistency of our pharmacophore strategy. Furthermore, the most potent compound from a series of BoNT/A LC SMNPIs reported by Park *et al.* (42) also mapped well to our expanded pharmacophore for BoNT/A LC inhibition (supplemental Fig. S2*A*). Even more compelling is fact that many of the key interactions that were modeled for this inhibitor (as shown in Fig. 2 of Ref. 42) are also predicted for docked models of mpp-RATKML and new SMNPIs from our study. This data further supports our common pharmacophore for BoNT/A LC inhibition, and demonstrates, for SMNPIs with very different molecular scaffolds, a clear convergence of functional/structural group interactions with critical residues in the substrate binding cleft of the enzyme. Likewise, our inhibitors, like those presented by Park *et al.* (42), were inactive when examined against the BoNT serotype B LC (data not shown).

NSC	K_i(μM)	Query Fit	Distances (Ang.) A-B[1]	A-C[1]	A-F[1]	Total[2]
341909	3.0		7.5	4.8	13.5	19.6
308574	6.0	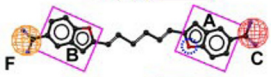	12.8	3.9	16.6	19.9
240898	10.0	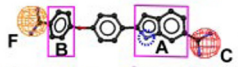	9.6	3.9	11.9	17.8
341907	10.0	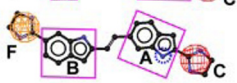	8.8	4.5	12.8	19.3

1 = Distances taken from planar centroids; 2 = Total length of the compounds

FIGURE 4. **Non-peptidic BoNT/A LC inhibitors: K_i values, search query mappings, and distances between pharmacophore components.** Colors are as indicated in the legend to Fig. 3, with the following modifications: pharmacophore component C is a *red mesh sphere* and the new polar ionizable component F is an *orange mesh sphere*.

During the molecular docking of our new inhibitors, good steric and chemical complementarity was observed when employing the same dynamic conformation of the BoNT/A LC that was pivotal for mpp-RATKML docking. Fig. 5, *A–C*, shows NSCs 341909, 308574, and 240898, respectively, docked in the BoNT/A LC substrate binding cleft. For all three inhibitors: 1) binding cleft occupancy is parallel to the longitudinal axis of the substrate binding cleft (with respect to enzyme orientation in the figure); 2) loop 1 serves as a solvent shield; 3) substituents that correspond to pharmacophore component C wedge between the side chain phenyls of Phe-162 and Phe-193); 4) a heteroatom associated with pharmacophore plane A, for example, the indole nitrogen of NSC 240898 (Fig. 5*C*), is positioned such that it may interfere with the catalytic engine of the enzyme; and 5) substituents that correspond to positive ionizable pharmacophore component F (Figs. 3*B* and 4) engage in hydrogen bonds with the side chain carboxylates of Glu-54 and Glu-63 (Fig. 5). Merino *et al.* (43) have reported highly flexible bis-imidazole inhibitors of the BoNT/A LC, and they too hypothesize that (like our polar ionizable pharmacophore component F) one of the imidazoles of their compounds engages in a hydrogen bond with the side chain carboxylate of Glu-54 (as indicated by Fig. 2 of Ref. 43). Again, the convergence of hypotheses for important inhibitor-enzyme residue contacts in the BoNT/A LC substrate binding cleft offers additional evidence supporting our structure-based pharmacophore approach. Recently, Boldt *et al.* (44) described an *o*,*p*-(dichloro)-cinnamic hydroxamate derivative that was indicated to inhibit the BoNT/A LC with an $IC_{50} = 0.41$ μM. However, when we tested this molecule under our assay conditions it possessed an IC_{50} of over 29 μM. These data are consistent with our hypothesis that increased substrate binding cleft occupancy,

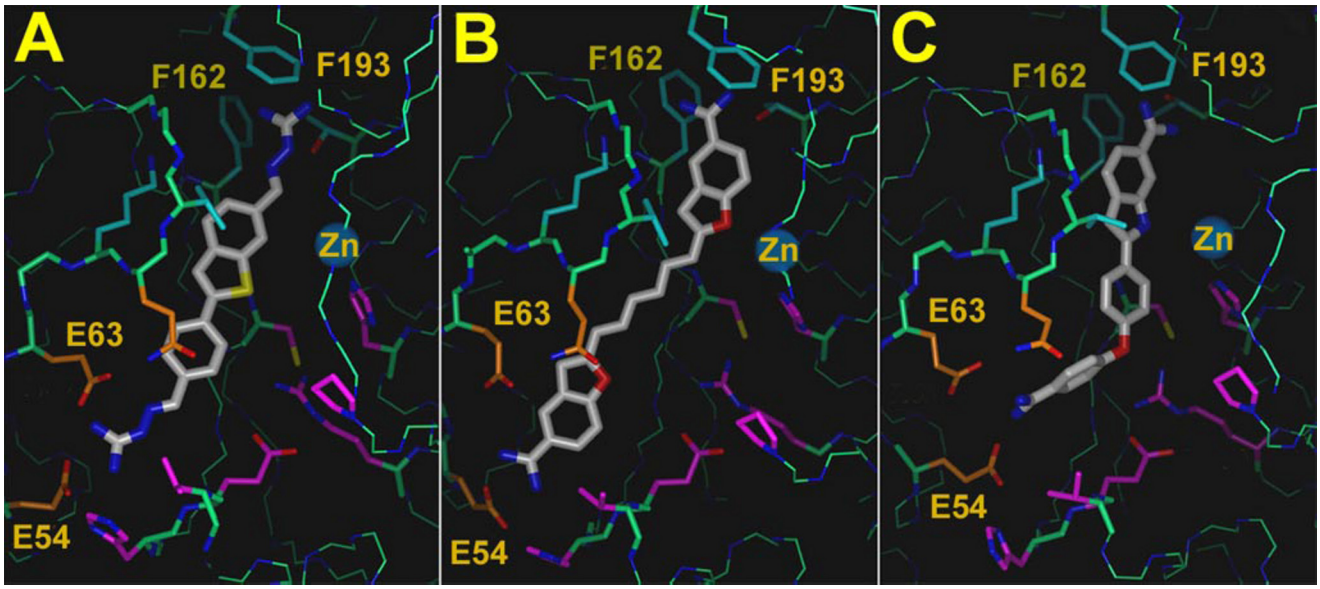

FIGURE 5. **Non-peptidic inhibitors docked in the BoNT/A LC conformation used for mpp-RATKML docking.** *Colors* and *stick thickness* are as indicated in the legends for Figs. 1, *A–D*, and 2, *A*, the inhibitors, NSC 341909 (*A*), NSC 308574 (*B*), and NSC 240898 (*C*), fit with good steric and hydropathic complementarity in the BoNT/A LC substrate binding cleft.

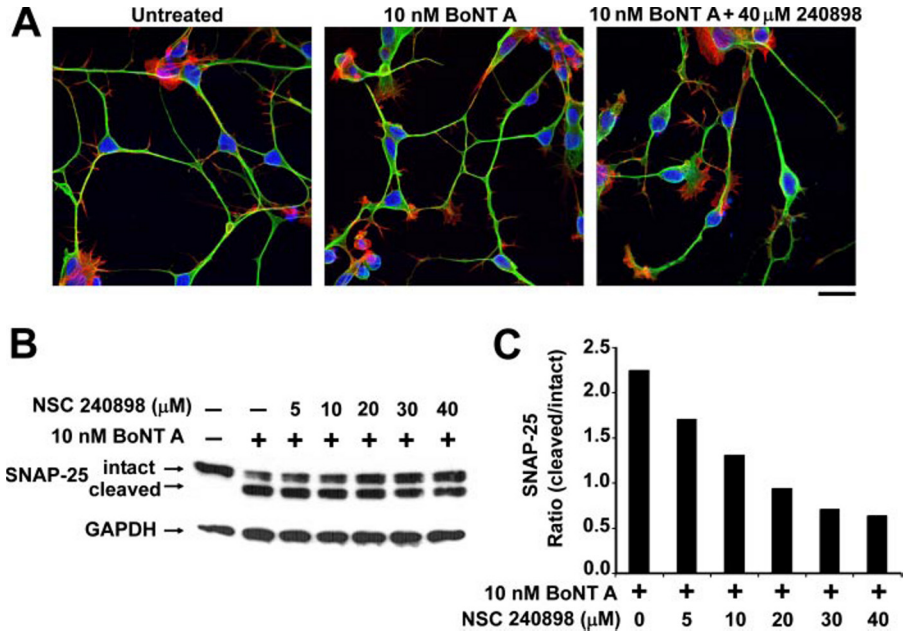

FIGURE 6. **NSC 240898 is well tolerated by neurons and is an effective inhibitor of BoNT/A LC-mediated cleavage of SNAP-25 in cells.** *A*, NSC 240898 lacks cytotoxic effects on chick spinal motor neurons. Staining for tubulin (*green*), actin filaments (*red*), and DNA (*blue*) show no gross morphological abnormalities in neurons after 3.5 h incubation with either 10 nM BoNT/A holotoxin or inhibitor + 10 nM BoNT/A holotoxin, when compared with untreated neurons. *Scale bar*, 20 μm. *B*, Western blot analysis reveals a dose-dependent inhibition of BoNT/A LC-mediated SNAP-25 cleavage in the presence of NSC 240898. *C*, densitometric scans of the bands in the Western blot are presented graphically as a ratio of cleaved to intact SNAP-25 for the concentrations of inhibitor tested.

TABLE 2

Measured and calculated thermodynamic values of NSC 240898 binding to the BoNT/A LC

	Thermodynamic value
Temperature (°C)	20
N[a]	0.83 ± 0.04
K_a (M^{-1})	$2.18 \times 10^5 \pm 4.5 \times 10^4$
K_d (μM)	4.6
ΔH (kcal mol^{-1})	−3.04 ± 0.20
ΔS (cal mol^{-1} K^{-1})	14.0

[a] The stoichiometry parameter (N) was adjusted in the fit in order to account for uncertainties in the concentration of protein in solution.

versus less, will increase inhibitor potency. Structurally, the dichloro-substituted phenyl of the Boldt *et al.* (44) compound corresponds to pharmacophore component C, the side chain alkene is pharmacophore plane A, and the hydroxamate moiety corresponds to a heteroatom (predicted to interfere with the BoNT/A LC catalytic engine) associated with plane A (supplemental Fig. S2*B*). Thus, this inhibitor also falls under the specifications of our pharmacophore for BoNT/A LC inhibition.

NSC 240898 Displays Dose-dependent Protection of SNAP-25 in a Neuronal Intoxication Assay—To be useful as therapeutics, the newly identified inhibitors must: 1) be able to enter neurons; 2) inhibit the toxin within the neuronal cytosol; and 3) be tolerated by the cells (*i.e.* possess acceptable toxicity profiles). We first tested inhibitors for neuronal uptake. Cultured chick spinal motor neurons were bathed in 20 μM inhibitor and examined by confocal microscopy to determine whether the autofluorescence of the compounds could be detected. Within 30 min three of the inhibitors became concentrated in the cells (supplemental Fig. S3). We next tested for potential cytotoxic effects by incubating the cells with various inhibitor concentrations for 3.5 h. Whereas NSCs 341909 and 308574 were cytotoxic at concentrations as low as 1–5 μM, NSC 240898 was well tolerated at concentrations as high as 40 μM. As shown in Fig. 6*A*, cells treated with 40 μM NSC 240898 for 3.5 h, fixed, and stained to show tubulin, actin filaments, and DNA revealed little or no morphological signs of damage (*e.g.* collapsed growth cones, abnormal axonal varicosities, or blebbing). Chick neurons were also exposed to 20 μM NSC 240898 for 24 h, and they remained as healthy as controls. Preincubation of cells for 30–45 min with varying concentrations of NSC 240898, followed by intoxication with 10 nM BoNT/A in the continued presence of inhibitor, demonstrated a dose-dependent inhibition of SNAP-25 cleavage in Western blot analyses (Fig. 6, *B* and *C*). These results indicate that NSC 240898 is a promising lead SMNPI, providing the foundation for the generation of a more potent derivative that may translate into a therapeutic. Furthermore, these findings also provide proof of concept that small drug-like molecules (in addition to described pseudo-peptides (45) and an amino acid derivative (46)), can be used as viable BoNT countermeasures.

Isothermal Titration Calorimetry—Because NSC 240898 demonstrated dose-dependent protection of SNAP-25 in a primary culture of embryonic chicken neurons, isothermal calorimetry experiments were conducted to further characterize the inhibitor interactions with the BoNT/A LC. Results from these studies (Table 2) indicated a low affinity binding event ($K_d \sim 4.6$ μM), with $n = 0.83 \pm 0.04$, which is consistent with a 1:1 stoichiometry (along with a small fraction of misfolded protein). Hence, as predicted by the model, NSC 240898 possesses a single binding site. Furthermore, the interaction was largely entropy-driven ($\Delta S = 14$ cal/mol K); comparatively, the enthalpic component was relatively low ($\Delta H = -3.04$ kcal/mol) (representative data are shown in Fig. 7). The substantial entropic contribution to the binding event suggests a burial of hydrophobic surfaces and the release of solvent. Taking into account the conformational variability of surface loops surrounding the BoNT/A LC substrate binding cleft, the observed solvent release is consistent with our hypothesis that the reorientation of these loops toward the substrate binding cleft facilitates the binding of mpp-RATKML and our SMNPIs.

Final Comments—A research strategy integrating molecular modeling (which adhered to empirical data and the fundamental principles of biochemically related sciences), pharmacophore-guided small molecule data base mining, *in vitro* and intra-

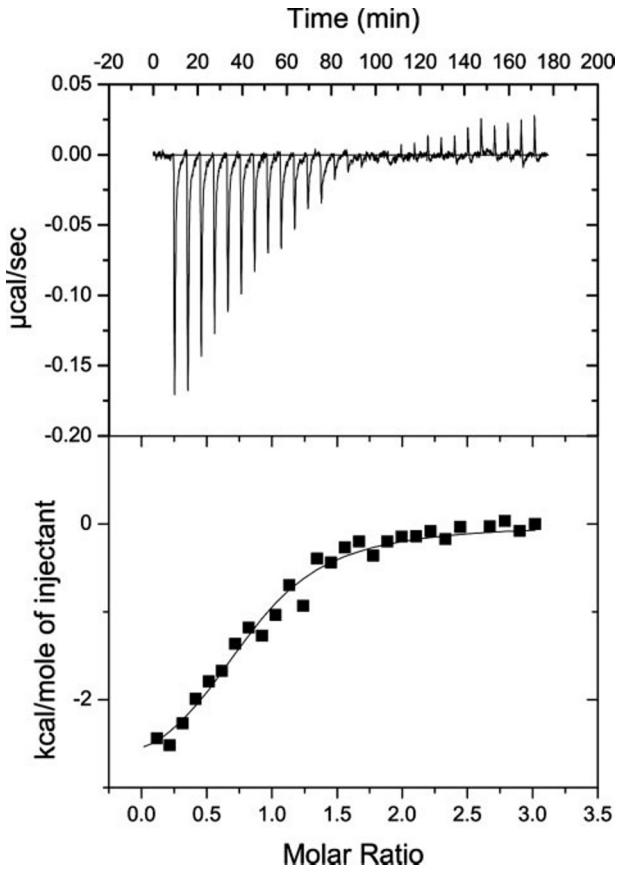

FIGURE 7. **Isothermal titration calorimetry of the NSC 240898-BoNT/A LC interaction.** *Top graph*, raw data obtained for 30 injections of 10 μl of 1.3 mM NSC 240898 solution into the sample cell containing 50 μM BoNT/A LC (after subtraction of the integration baseline). *Bottom graph*, normalized integrated enthalpies plotted against the molar ratio NSC 240898: BoNT/A LC. The *solid line* corresponds to the best fit curve obtained by non-linear least square fit minimization. The binding followed a 1:1 stoichiometry and is largely entropy-driven. Due to the low affinity of the interaction, a large excess of the inhibitor was necessary to drive the titration to saturation. Protein concentration was determined by amino acid analysis (Molecular Structure Facility, University of California, Davis, CA), and NSC 240898 concentration was confirmed by UV-visible absorbance measurements.

cellular biological testing, and cellular visualization was used to successfully identify a lead candidate for therapeutic development. The importance of identifying a binding mode for mpp-RATKML was underscored by the fact that we were able to use the docked conformation of the pseudo-peptide to generate a data base search query that chemoinformatically identified new and more potent SMNPIs. Of these, NSC 240898 showed dose-dependent protection of SNAP-25 cleavage in primary cultures of embryonic chicken spinal motor neurons and displayed no cellular toxicity, even at a high 40 μM concentration. Hence, this compound provides a viable lead molecular scaffold for the further development of a therapeutic countermeasure.

Acknowledgments—We thank Dr. Daqi Tu, Dr. Alex Bankovich, and Edna Torres-Melendez for technical assistance. We thank the National Cancer Institute for providing compounds and for the allocation of computing time and staff support at the Advanced Biomedical Computing Center of the Frederick Cancer Research and Development Center.

REFERENCES

1. Paddle, B. M. (2003) *J. Appl. Toxicol.* **23,** 139–170
2. Burnett, J. C., Henchal, E. A., Schmaljohn, A. L., and Bavari, S. (2005) *Nat. Rev. Drug Discov.* **4,** 281–297
3. Josko, D. (2004) *Clin. Lab. Sci.* **17,** 30–34
4. Clarke, S. C. (2005) *Br. J. Biomed. Sci.* **62,** 40–46
5. Lipozencic, J., and Bukvic Mokos, Z. (2006) *Acta Dermatovenerol. Croat.* **14,** 60
6. Marks, J. D. (2004) *Anesthesiol. Clin. North America* **22,** vii, 509–532
7. Montecucco, C., and Molgo, J. (2005) *Curr. Opin. Pharmacol.* **5,** 274–279
8. Cheng, C. M., Chen, J. S., and Patel, R. P. (2006) *Am. J. Health Syst. Pharm.* **63,** 225–232
9. Cote, T. R., Mohan, A. K., Polder, J. A., Walton, M. K., and Braun, M. M. (2005) *J. Am. Acad. Dermatol.* **53,** 407–415
10. Meunier, F. A., Lisk, G., Sesardic, D., and Dolly, J. O. (2003) *Mol. Cell. Neurosci.* **22,** 454–466
11. Lacy, D. B., Tepp, W., Cohen, A. C., DasGupta, B. R., and Stevens, R. C. (1998) *Nat. Struct. Biol.* **5,** 898–902
12. Dong, M., Yeh, F., Tepp, W. H., Dean, C., Johnson, E. A., Janz, R., and Chapman, E. R. (2006) *Science* **312,** 592–596
13. Singh, B. R. (2000) *Nat. Struct. Biol.* **7,** 617–619
14. Binz, T., Blasi, J., Yamasaki, S., Baumeister, A., Link, E., Sudhof, T. C., Jahn, R., and Niemann, H. (1994) *J. Biol. Chem.* **269,** 1617–1620
15. Schiavo, G., Benfenati, F., Poulain, B., Rossetto, O., Polverino de Laureto, P., DasGupta, B. R., and Montecucco, C. (1992) *Nature* **359,** 832–835
16. Schiavo, G., Malizio, C., Trimble, W. S., Polverino de Laureto, P., Milan, G., Sugiyama, H., Johnson, E. A., and Montecucco, C. (1994) *J. Biol. Chem.* **269,** 20213–20216
17. Schiavo, G., Rossetto, O., Catsicas, S., Polverino de Laureto, P., DasGupta, B. R., Benfenati, F., and Montecucco, C. (1993) *J. Biol. Chem.* **268,** 23784–23787
18. Schiavo, G., Shone, C. C., Rossetto, O., Alexander, F. C., and Montecucco, C. (1993) *J. Biol. Chem.* **268,** 11516–11519
19. Blasi, J., Chapman, E. R., Yamasaki, S., Binz, T., Niemann, H., and Jahn, R. (1993) *EMBO J.* **12,** 4821–4828
20. Smith, T. J., Lou, J., Geren, I. N., Forsyth, C. M., Tsai, R., Laporte, S. L., Tepp, W. H., Bradshaw, M., Johnson, E. A., Smith, L. A., and Marks, J. D. (2005) *Infect. Immun.* **73,** 5450–5457
21. Schmidt, J. J., and Stafford, R. G. (2002) *FEBS Lett.* **532,** 423–426
22. Schmidt, J. J., Stafford, R. G., and Bostian, K. A. (1998) *FEBS Lett.* **435,** 61–64
23. Nguyen, T. L., McGrath, C., Hermone, A. R., Burnett, J. C., Zaharevitz, D. W., Day, B. W., Wipf, P., Hamel, E., and Gussio, R. (2005) *J. Med. Chem.* **48,** 6107–6116
24. Giannakakou, P., Gussio, R., Nogales, E., Downing, K. H., Zaharevitz, D., Bollbuck, B., Poy, G., Sackett, D., Nicolaou, K. C., and Fojo, T. (2000) *Proc. Natl. Acad. Sci. U. S. A.* **97,** 2904–2909
25. Segelke, B., Knapp, M., Kadkhodayan, S., Balhorn, R., and Rupp, B. (2004) *Proc. Natl. Acad. Sci. U. S. A.* **101,** 6888–6893
26. Burnett, J. C., Schmidt, J. J., McGrath, C. F., Nguyen, T. L., Hermone, A. R., Panchal, R. G., Vennerstrom, J. L., Kodukula, K., Zaharevitz, D. W., Gussio, R., and Bavari, S. (2005) *Bioorg. Med. Chem.* **13,** 333–341
27. Burnett, J. C., Schmidt, J. J., Stafford, R. G., Panchal, R. G., Nguyen, T. L., Hermone, A. R., Vennerstrom, J. L., McGrath, C. F., Lane, D. J., Sausville, E. A., Zaharevitz, D. W., Gussio, R., and Bavari, S. (2003) *Biochem. Biophys. Res. Commun.* **310,** 84–93
28. Breidenbach, M. A., and Brunger, A. T. (2004) *Nature* **432,** 925–929
29. Alberts, I. L., Nadassy, K., and Wodak, S. J. (1998) *Protein Sci.* **7,** 1700–1716
30. Roe, R. R., and Pang, Y. P. (1999) *J. Mol. Model.* **5,** 134–140
31. Schmidt, J. J., and Bostian, K. A. (1995) *J. Protein Chem.* **14,** 703–708
32. Schmidt, J. J., and Bostian, K. A. (1997) *J. Protein Chem.* **16,** 19–26
33. Segel, I. H. (1975) *Enzyme Kinetics*, Wiley, New York
34. Kuhn, T. B. (2003) *Methods Cell Biol.* **71,** 67–87
35. Schmidt, J. J., and Stafford, R. G. (2003) *Appl. Environ. Microbiol.* **69,** 297–303
36. Sukonpan, C., Oost, T., Goodnough, M., Tepp, W., Johnson, E. A., and

Rich, D. H. (2004) *J. Pept. Res.* **63,** 181–193
37. Swaminathan, S., Eswaramoorthy, S., and Kumaran, D. (2004) *Mov. Disord.* **19,** Suppl. 8, S17–S22
38. Kukreja, R., and Singh, B. (2005) *J. Biol. Chem.* **280,** 39346–39352
39. Flocco, M. M., and Mowbray, S. L. (1994) *J. Mol. Biol.* **235,** 709–717
40. Borders, C. L., Jr., Broadwater, J. A., Bekeny, P. A., Salmon, J. E., Lee, A. S., Eldridge, A. M., and Pett, V. B. (1994) *Protein Sci.* **3,** 541–548
41. Mitchell, J. B., Nandi, C. L., McDonald, I. K., Thornton, J. M., and Price, S. L. (1994) *J. Mol. Biol.* **239,** 315–331
42. Park, J. G., Sill, P. C., Makiyi, E. F., Garcia-Sosa, A. T., Millard, C. B., Schmidt, J. J., and Pang, Y. P. (2006) *Bioorg. Med. Chem.* **14,** 395–408
43. Merino, I., Thompson, J. D., Millard, C. B., Schmidt, J. J., and Pang, Y. P. (2006) *Bioorg. Med. Chem*. **14,** 3583–3591
44. Boldt, G. E., Kennedy, J. P., and Janda, K. D. (2006) *Org. Lett.* **8,** 1729–1732
45. Anne, C., Turcaud, S., Blommaert, A. G., Darchen, F., Johnson, E. A., and Roques, B. P. (2005) *Chembiochem* **6,** 1375–1380
46. Boldt, G. E., Eubanks, L. M., and Janda, K. D. (2006) *Chem. Commun.* **29,** 3063–3065